Preliminary Experience With Intraoperative Near-infrared Fluorescence Imaging in Percutaneous Sclerotherapy of Soft-Tissue Venous Malformations

KOSUKE ISHIKAWA, MD,* SATORU SASAKI, MD, PHD,* HIROSHI FURUKAWA, MD, PHD,† MUNETOMO NAGAO, MD, PHD,* DAISUKE IWASAKI, MD,* NORIKO SAITO, MD, PHD,* AND YUHEI YAMAMOTO, MD, PHD†

BACKGROUND It has recently been demonstrated that near-infrared (NIR) fluorescence imaging can be used to visualize the blood vasculature. Although sclerotherapy has been successfully used in treating venous malformations, the spread of sclerosant is difficult to monitor during sclerotherapy.

OBJECTIVE To evaluate the safety and efficacy of NIR fluorescence imaging in percutaneous sclerotherapy of soft-tissue venous malformations.

METHODS AND MATERIALS The use of NIR fluorescence imaging after administration of indocyanine green (ICG) was evaluated in duplex-guided sclerotherapy performed on 15 patients with venous malformations. The lower extremities were involved in seven, the upper extremities in four, and the face in four.

RESULTS In 13 of the 15 procedures, spotty fluorescence images were obtained, and in eight procedures, linear fluorescence images were obtained. In two patients with intramuscular venous malformations in the lower extremities, no fluorescence images were obtained. Observational depth seemed to be <1 cm below the skin surface with an ICG concentration of 0.01 mg/mL. No complications associated with ICG were observed. Adjacent tissue ulceration occurred in one patient.

CONCLUSION NIR fluorescence imaging with ICG can be a useful additional monitor for percutaneous sclerotherapy of venous malformations, especially in the face and hands, enabling noninvasive assessment of real-time spread of sclerosant.

The authors have indicated no significant interest with commercial supporters.

Sclerotherapy has been a useful alternative to surgical excision of vascular malformations.[1,2] One of the most common causes of complications during the procedure is extravasation of sclerosant, with necrosis of adjacent tissue.[3] Therefore, procedural guidance is required to ensure precise puncture, and the spread of sclerosant should be carefully monitored. Various sclerotherapy techniques have been reported: fluoroscopic guided,[3] duplex guided,[4] and magnetic resonance (MR) guided.[5] Recently near-infrared (NIR) fluorescence imaging has been demonstrated to offer real-time visualization, enabling noninvasive assessment of lymphatic and blood vasculature.[6] Kikuchi and Hosokawa reported that intraoperative NIR fluorescence imaging allowed for visualization of sclerosant spreading in varicose veins.[7] We used a real-time NIR fluorescence imaging system with indocyanine green (ICG) as an additional monitor of the spread of sclerosant in duplex-guided percutaneous sclerotherapy of soft-tissue venous malformations. In this report, we describe our clinical experience and evaluate the safety and efficacy of NIR fluorescence imaging.

**Center for Vascular Anomalies, KKR Sapporo Medical Center Tonan Hospital, Sapporo, Japan; †Department of Plastic and Reconstructive Surgery, Hokkaido University Graduate School of Medicine, Sapporo, Japan*

ISSN: 1076-0512 • Dermatol Surg 2013;39:907–912 • DOI: 10.1111/dsu.12152

Patients

The use of NIR fluorescence imaging was evaluated in duplex-guided percutaneous sclerotherapy performed on 15 patients (ages 3–64, average 14.9) with venous malformations from March to August 2010 at KKR Sapporo Medical Center Tonan Hospital. The lower extremities were involved in seven, the upper extremities in four, and the face in four. Before the procedure, all patients underwent color duplex ultrasound and MR imaging to evaluate the extent, distribution, and character of the lesions. The diagnosis of a venous malformation was made on the basis of clinical history, physical examination, ultrasound, and MR imaging. The lesions of all patients in the study met the MR imaging criteria for venous malformations.[8] Follow-up ranged from 1 to 16 months (average 6.3 months). This study conformed to the ethical guidelines of the 1975 Declaration of Helsinki.

Methods

NIR Fluorescence Imaging

Intraoperatively, venous malformations were visualized through direct injection of a solution of ICG and sclerosant using a NIR fluorescence camera device [Photodynamic Eye (PDE); Hamamatsu Photonics K.K., Shizuoka, Japan] equipped with 760-nm light-emitting diodes within a handheld unit with a charge-coupled device camera as a detector and a bandpass filter to block light below 820 nm.[6] The maximum excitation and fluorescence wavelengths of ICG in plasma are 765 nm and 840 nm, respectively.[9] Fluorescence within the NIR spectral range ($\geq$ 800 nm) is tissue penetrating, and the PDE provides noninvasive detection of the fluorescence in deeper tissues. This device is portable and easy to use intraoperatively. The fluorescence signals were digitalized for real-time display in monochrome. According to the recorded movies of the procedures, patterns of fluorescence images were classified as linear images, spotty images, or no images obtained. Linear images were defined as more than one vessel-like fluorescence pattern originating from spotty images, which were defined as a local dim fluorescence pattern.

ICG and Sclerosants

ICG (Diagnogreen for injection; Daiichi-Sankyo Co. Ltd., Tokyo, Japan) was used as an NIR fluorophore. Concentrated ICG solution (0.04 mL) was made by dissolving ICG (25 mg) in injection solvent (10 mL) and added to 10 mL of sclerosant solution, resulting in an ICG concentration of 0.01 mg/mL.[7] The sclerosants were absolute ethanol and 3% polidocanol (Polidocasklerol 3% injection; Zeria Pharmaceutical Co., Ltd., Tokyo, Japan) foamed using the Tessari method.[10] The stable sclerosing microfoam was obtained by mixing 2 mL of polidocanol with atmospheric air at a 1:4 ratio in two syringes attached using a three-way stopcock.

Procedures

All patients were treated under general anesthesia. Direct puncture of the venous malformation was performed using a 22-G angiocatheter with color duplex ultrasound (LOGIQ e; GE Yokogawa Medical Co., Ltd., Tokyo, Japan) to visualize needle placement and facilitate direct cannulation of the vascular channels. Then sclerosant solution mixed with ICG was slowly injected under duplex guidance, and fluorescence images were obtained through the PDE held 15–20 cm from the skin surface to monitor the spread of sclerosant. Operating lights were turned off during the procedure, and room lights were left on to keep light reflection off the skin. In most patients, direct puncture and sclerosis were performed in more than one region of the venous malformation. The sclerotherapy was stopped when the vascular lesion was sufficiently filled according to duplex sonography, when the use of sclerosants reached a maximum dose of 1 mL/kg, or when fluorescence images were obtained at the contralateral side of the treated finger.

Results

Patient characteristics, treatments, and outcomes are summarized in Table 1. Spotty fluorescence images

TABLE 1. Patient Characteristics, Treatments and Outcomes

Patient			*Venous Malformation*				
No.	*Age*	*Sex*	*Location*	*Distribution*	*Treated region*	*Sclerosant*	*Pattern of Fluorescence Images*
1	7	Male	SC	Upper extremity	Hand	POL	Linear
2	17	Male	SC	Face	Lip	ET	Spotty
3	11	Male	IM	Lower extremity	Thigh	ET	None obtained
4	7	Female	SC	Lower extremity	Thigh	ET	Spotty
5	15	Female	SC	Lower extremity	Thigh, buttock	ET	Linear
6	11	Female	SC	Lower extremity	Buttock	ET, POL	Spotty
7	17	Female	IM	Lower extremity	Leg	ET	None obtained
8	6	Female	SC	Upper extremity	Fingers	POL	Linear
9	11	Female	SC	Face	Cheek	ET	Linear
10	17	Female	SC	Upper extremity	Thumb	ET	Linear
11	9	Male	SC	Lower extremity	Leg	POL	Spotty
12	3	Male	SC	Lower extremity	Foot	ET, POL	Spotty
13	64	Female	SC	Face	Lower eyelid	POL	Linear
14	6	Female	SC	Upper extremity	Finger	POL	Linear
15	22	Female	SC	Face	Lip	ET, POL	Linear

SC, subcutaneous; IM, intramuscular; POL, polidocanol; ET, ethanol.

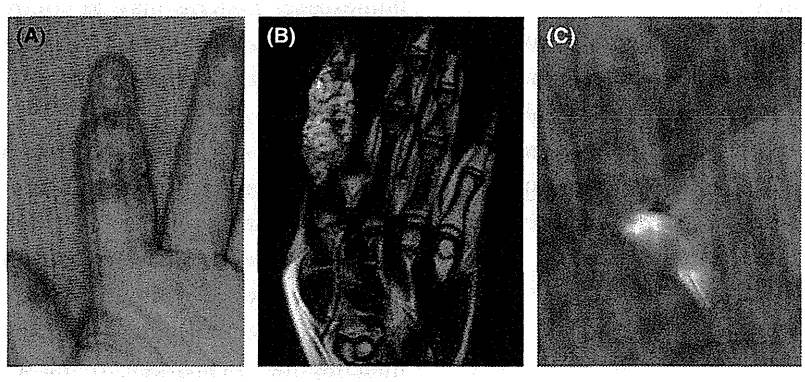

Figure 1. Case 14. Patient with venous malformation in the left index finger. (A) Preoperative view of the left hand. (B) Coronal fat-suppressed T2-weighted magnetic resonance image obtained before sclerotherapy shows a homogenous hyperintense mass in the left index finger. (C) Fluorescence image obtained during sclerotherapy shows unilateral contrast of the treated region of the index finger. Sclerotherapy was stopped when fluorescence images were obtained at the contralateral side of the index finger.

were obtained from the skin surface in 13 of the 15 procedures (87%) and linear fluorescence images in eight (53%). No fluorescence images were obtained in two patients with intramuscular venous malformations in the lower extremities. These intramuscular lesions were located more than 1 cm below the skin surface. Image quality and spatial resolution on PDE were sufficient for visualization of ICG and sclerosant spread. In two procedures (patients 8 and 14), NIR fluorescence imaging was useful in deciding when to stop the sclerotherapy because fluorescence images were obtained at the contralateral side of the treated finger (Figure 1). Linear fluorescence images were more likely to be obtained in the upper extremities and the face than in the lower extremities (Table 2). Linear images seemed to represent the flow in draining vessels, and spotty images seemed to represent the intralesional or extralesional existence of ICG. Fluorescence images were obtained at the end of the procedure, which

TABLE 2. Evaluation of Pattern of Fluorescence Images in 15 Patients

Distribution of Venous Malformations	Pattern n		
	Linear Images	Spotty Images	None Obtained
Upper extremity	4		
Lower extremity	1	4	2
Face	3	1	

took approximately 30 minutes, without a decrease in fluorescence. No worsening of the initial clinical situation occurred, and no complications associated with ICG were observed. The volume of ethanol used per treatment session ranged from 0.8 to 36.2 mL (average 14.3 mL) and that of foam polidocanol from 4.0 to 19.8 mL (average 8.5 mL). A local complication occurred as a result of the procedure in one of the 15 procedures. Intraoral ulceration occurred in a 17-year-old man (patient 2) with an extensive venous malformation of the face who had undergone ethanol sclerotherapy of the lip but eventually healed. No other complications, such as cutaneous necrosis, damage to local nerve, and symptomatic embolism of the sclerosant into the circulation, were observed during follow-up.

Discussion

Percutaneous sclerotherapy has been established as a minimally invasive treatment option for slow-flow vascular malformations.[2] The combination of sonographic and fluoroscopic guidance increases the safety of the procedure by allowing direct imaging of venous drainage.[3] Duplex sonography has been described as a real-time guidance technique providing visualization of the extent of the malformation and assessment of blood flow velocity.[4] MR-guided sclerotherapy allows direct visualization of needle placement and sclerosant distribution.[5] The value of navigation guidance for percutaneous sclerotherapy is based on the additional information derived from visualization of the target lesion. Several recent investigational studies have used NIR fluorescence imaging system after administration of ICG for intraoperative identification of lymph nodes and patency of lymph and blood vessels, as well as noninvasive assessment of lymphatic function.[6,11]

Duplex-guided sclerotherapy has been our standard method for the treatment of venous malformations. In this trial, we used real-time NIR fluorescence imaging as an additional monitor of the spread of sclerosant intraoperatively. Although observation on duplex sonography is limited to the cross-sectional area contacted by the probe, NIR fluorescence imaging can visualize sclerosant spreading horizontally on the skin surface. Nevertheless, extravasation of the ICG–sclerosant solution may cause visualization of extravascular space. Given that ICG binds to globulin proteins within tissues, it may be taken up by the lymphatics and visualize lymphatic vessels unexpectedly. Visual interpretation of the spotty fluorescence patterns may be controversial if they reflect intravascular spread or extravasation of sclerosant in this series.

Owing to its sensitivity, fluoroscopic imaging with radiopaque contrast medium is the clinical standard for vascular imaging, but NIR fluorescence imaging may provide noninvasive visualization that can be repeatedly excited without radiation exposure. There is also an advantage for NIR fluorescence imaging that is enhanced by the smaller amounts of contrast agent than with MR- or computed tomography–based angiography procedures.[6] Depth of penetration of NIR fluorescence is estimated to be between 2 and 3 cm below the skin surface.[7] In this series, observational depth seemed to be <1 cm below the skin surface with an ICG concentration of 0.01 mg/mL.

For sclerotherapy of venous malformations, especially those in the face and hands, the risk of necrosis should be carefully considered from an esthetic point of view. Linear fluorescence images were obtained more often in these regions (Table 2), because it was assumed that subcutaneous tissue was thin and vascular vessels well-developed.

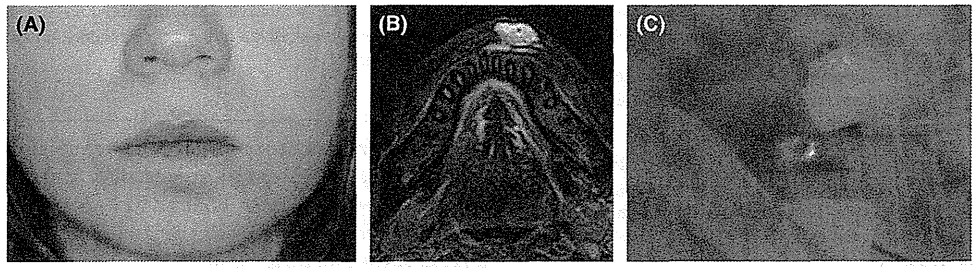

Figure 2. Case 15. Patient with venous malformation in the lower lip. (A) Preoperative view of the face. (B) Axial fat-suppressed T2-weighted magnetic resonance image obtained before sclerotherapy shows a homogenous hyperintense mass in the lower lip. (C) Fluorescence image obtained during sclerotherapy shows the spread of sclerosant in the lower lip.

Because of the limits of its tissue-penetrating depth, NIR fluorescence imaging can be suitable for lesions located in the face and hands (Figures 1 and 2). For lesions located in the fingers, the flow of sclerosant to the contralateral side of the treated finger could lead to total necrosis of the finger. In duplex-guided sclerotherapy, it is difficult to monitor the spread of sclerosant in the whole finger. NIR fluorescence imaging made it possible to detect flow to the contralateral side of the treated finger.

ICG is a tricarbocynanine dye that has been used clinically for longer than 50 years for hepatic clearance, cardiovascular function testing, and retinal angiography on the basis of its dark green color. ICG associates with albumin, making it an excellent vascular agent for evaluating the blood and lymphatic systems.[6] Most studies have used NIR fluorescence imaging systems after administration of mg amounts of ICG.[6,11] Our ICG concentration of 0.01mg/mL was enough to get visualization of sclerosant spreading. The incidence of adverse reactions related to ICG injection was reported to be 0.4%, and 0.05% for severe adverse reactions such as hypotension, arrhythmia, and anaphylactic shock.[12] No suspended matter was found in the mixture of ICG with absolute ethanol or 3% polidocanol, and the mixed solution was stable.

NIR fluorescence images with ICG were obtained in 13 of 15 procedures (87%) without any complications associated with ICG. This technique of NIR fluorescence imaging is safe and noninvasive. The device is portable and easy to use, and real-time fluorescence images can be obtained. The combination of duplex sonography and NIR fluorescence imaging may provide safer, more-efficient sclerotherapy. Although further study is necessary to validate the results of this trial, this method can be used as a useful additional monitor for sclerotherapy of venous malformations, especially those located in the face and hands.

References

1. Yakes WF, Haas DK, Parker SH, Gibson MD, et al. Symptomatic vascular malformations: ethanol embolotherapy. Radiology 1989;170:1059–66.
2. Berenguer B, Burrows PE, Zurakowski D, Mulliken JB. Sclerotherapy of craniofacial venous malformations: complications and results. Plast Reconstr Surg 1999;104:1–11.
3. Donnelly LF, Bissett GS 3rd, Adams DM. Combined sonographic and fluoroscopic guidance: a modified technique for percutaneous sclerosis of low-flow vascular malformations. AJR Am J Roentgenol 1999;173:655–7.
4. Yamaki T, Nozaki M, Sasaki K. Color duplex-guided sclerotherapy for the treatment of venous malformations. Dermatol Surg 2000;26:323–8.
5. Hayashi N, Masumoto T, Okubo T, Abe O, et al. Hemangiomas in the face and extremities: MR-guided sclerotherapy-optimization with monitoring of signal intensity changes in vivo. Radiology 2003;226:567–72.
6. Marshall MV, Rasmussen JC, Tan I-C, Aldrich MB, et al. Near-infrared fluorescence imaging in humans with indocyanine green: a review and update. Open Surg Oncol J 2010;2:12–25.
7. Kikuchi M, Hosokawa K. Visualized sclerotherapy of varicose veins. Dermatol Surg 2010;36(Suppl 2):1050–5.
8. Meyer JS, Hoffer FA, Barnes PD, Mulliken JB. Biological classification of soft-tissue vascular anomalies: MR correlation. AJR Am J Roentgenol 1991;157:559–64.

9. Benson RC, Kues HA. Fluorescence properties of indocyanine green as related to angiography. Phys Med Biol 1978;23:159–63.

10. Tessari L, Cavezzi A, Frullini A. Preliminary experience with a new sclerosing foam in the treatment of varicose veins. Dermatol Surg 2001;27:58–60.

11. Furukawa H, Osawa M, Saito A, Hayashi T, et al. Microsurgical lymphaticovenous implantation targeting dermal lymphatic backflow using indocyanine green fluorescence lymphography in the treatment of postmastectomy lymphedema. Plast Reconstr Surg 2011;127:1804–11.

12. Hope-Ross M, Yannuzzi LA, Gragoudas ES, Guyer DR, et al. Adverse reactions due to indocyanine green. Ophthalmology 1994;101:529–33.

Address correspondence and reprint requests to: Satoru Sasaki, MD, PhD, Center for Vascular Anomalies, KKR Sapporo Medical Center Tonan Hospital, Kita 1, Nishi 6, Chuou-ku, Sapporo 060–0001, Japan, or
e-mail: satoru-s@tonan.gr.jp

Journal of Tissue Viability (2013) 22, 103–111

ELSEVIER

JOURNALOF tissueviability

www.elsevier.com/locate/jtv

Review

Vascular anomalies and wounds

Sadanori Akita*, Seiji Houbara, Mihoko Akatsuka, Akiyoshi Hirano

Department of Plastic Surgery, Nagasaki University Hospital, 1-7-1 Sakamoto, Nagasaki 8538501, Japan

KEYWORDS
Vascular anomaly;
Vascular tumour;
Vascular malformation;
Ulcer;
Necrosis

Abstract Vascular anomalies comprise vascular tumours and vascular malformations. Some vascular anomalies result in ulcerations and necrosis. In vascular tumours, infantile haemangiomas are predominant and ulceration is demonstrated in up to 16%. In vascular malformations, arteriovenous malformations predominate and frequently demonstrate either primary ulceration or skin necrosis after diagnostic and therapeutic procedures. Various diagnostic and therapeutic imaging methods, such as X-ray, computed tomography (CT), magnetic resonance imaging (MRI), duplex Doppler ultrasound, and angiography, are used to visualize vascular anomalies; angiograms are required when embolization is attempted and blood flow needs to be further investigated. Duplex Doppler ultrasound is useful for routine check-ups as a therapeutic tool; however, it has limited in precision and accuracy. The aim of the present review is to give an overview of wounds related to vascular anomalies, detailing the diagnostic imaging and treatment options.

Introduction

Vascular anomalies comprise two distinct main types: vascular tumours and vascular malformations. Vascular malformations include capillary malformation (CM), venous malformation (VM), lymphatic malformation (LM), and arteriovenous malformation (AVM) [1], and are distinct from vascular tumours regarding clinical appearance, imaging, and histopathological characteristics [2]. Vascular tumours mainly comprise infantile haemangioma (IH) and other related rare vascular tumours, such as congenital haemangiomas (rapidly involuting congenital haemangioma, RICH or non-involuting congenital haemangioma, NICH), kaposiform haemangioendothelioma, tufted angioma, pyogenic granuloma, and haemangiopericytoma in children and in adults.

Various imaging methods, such as ultrasound, magnetic resonance imaging (MRI), computed tomography (CT), and angiography, are employed in the diagnosis of vascular tumours and vascular malformations. The selection of these techniques is based on the clinical findings and the aim of imaging, i.e., diagnostic, pre- and intra-treatment assessment, or follow-up.

The present review reflects the authors' experience with from January 2006 to March 2012, in which 231 cases of vascular anomalies (201 cases

* Corresponding author.
E-mail address: akitas@hf.rim.or.jp (S. Akita).

0965-206X/$36
http://dx.doi.org/10.1016/j.jtv.2013.08.001

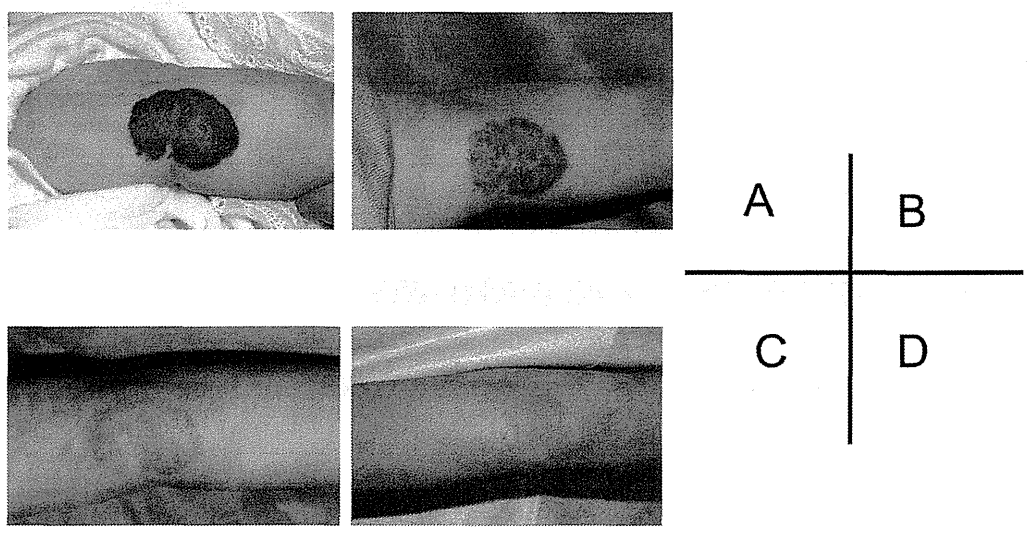

Figure 1 Typical IH in the elbow. A: At 4 months old, appearance of the lesion at the first visit. B: At 1.5 years of age, the redness has decreased. C: At 2.5 years of age, the colour has become much fainter. D: At 6 years of age, the colour has completely regressed and the skin shows some anetoderma. (For interpretation of the references to colour in this figure legend, the reader is referred to the web version of this article.)

were vascular malformations and 30 cases were haemangiomas) were treated in the Department of Plastic and Reconstructive Surgery, Nagasaki University Hospital. Among the cases of vascular malformations, the number of patients with VMs, AVMs, LMs, lymphatico-venous malformations (LVMs), capillary malformations (CMs), capillary-venous malformations (CVMs), arteriovenous-lymphatic malformation (AVLMs) was 114, 43, 17, 9, 9, 5, and 4, respectively. Of the haemangiomas, 28 cases were IHs and two were congenital haemangiomas (mean age: 32.6 ± 22.76; range; 3 months to 88 years). There were seven cases of primary ulceration in 201 vascular malformations and two in 30 cases of haemangiomas. All treatments in this clinical series were approved by the Internal Review Board of Nagasaki University (approved number 10032690) and informed consent was obtained.

IH

The majority of IHs are small and not hazardous, may recede spontaneously with proliferation, involution, and involuted phases. IH can be alarming if they occur at life- and function-threatening locations, such as the eyelid, orbit,

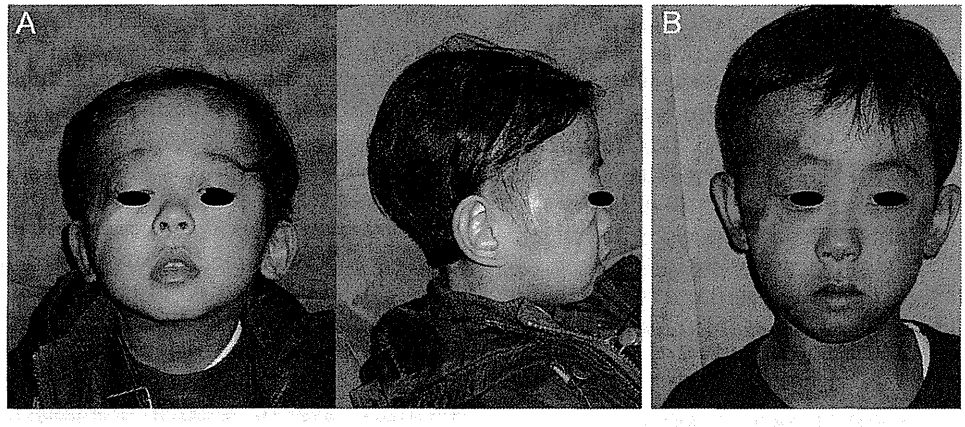

Figure 2 Healed IH. A: Photograph of a 2-year-old child with IH in the right eyelid, temporal area, and cheek, which shows laxity and shrinkage of the skin overhanging the eye at first visit. B: At 6 years after surgical removal of the lax skin and anetoderma.

Figure 3 NICH in a child at 7 months (left) and at 4 years of age (right). Clinical manifestations remained over the 3-year period.

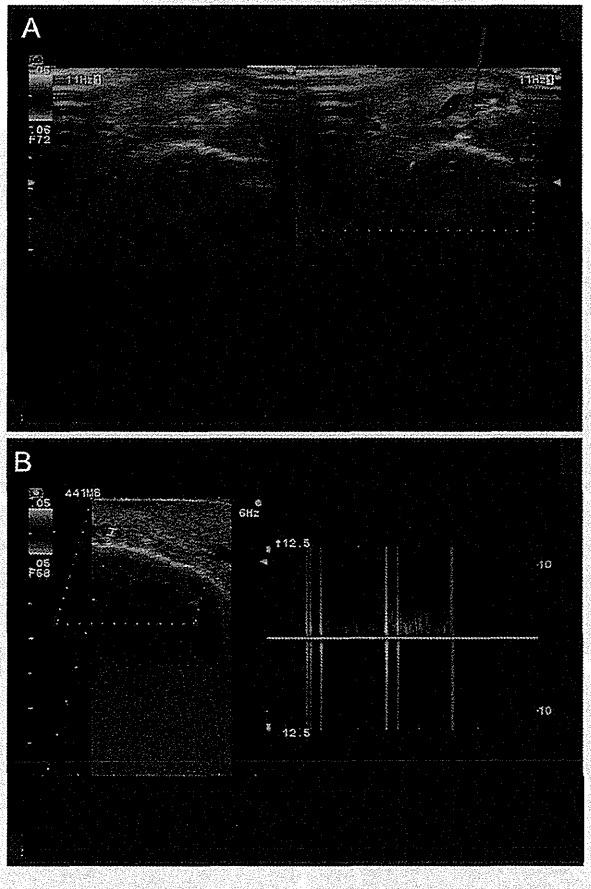

Figure 4 Duplex Doppler ultrasound. A: In-flow view, the hypervascularity of in- and out-flows is observed, as frequently seen in AVMs (arrow). B: Doppler mode demonstrates fast shunt flow. Progression of IH in the left elbow joint at 4 months in the first visit (left) and at 6 years (right).

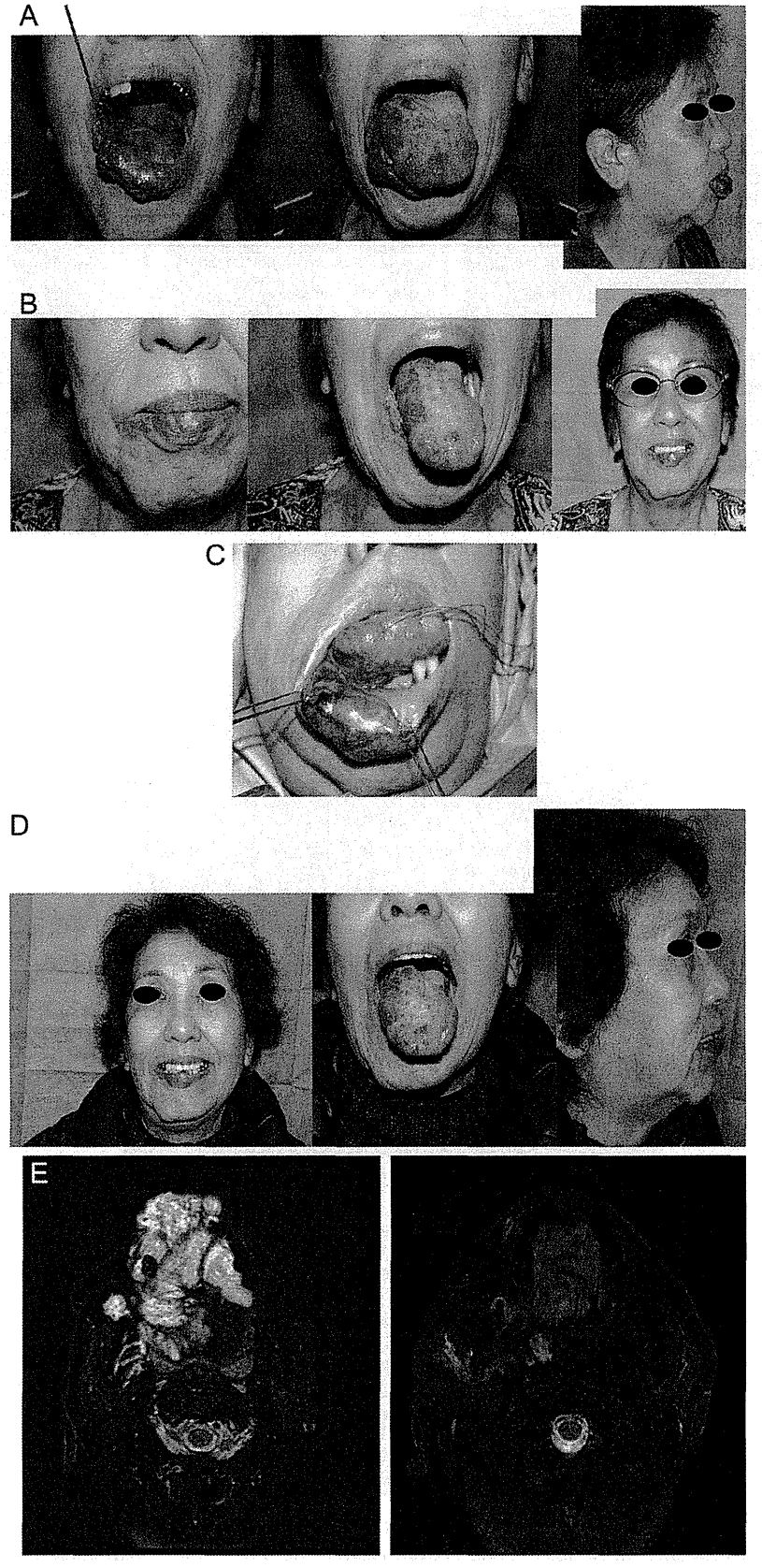
A
B
C
D
E

or airway. In those cases involving ulceration, continued infection, or haemorrhage treatment is required. Ulceration is one of the most common complications of IH. The incidence in a referral population is generally reported to be approximately 16%. A prospective study of 1096 patients reported the median age at ulceration was 4 months, which correlates with the end of the proliferative phase [3]. Risk factors for ulceration include segmental morphological characteristics, large size, and mixed superficial and deep subtypes. Early white discolouration may suggest impending ulceration [4]. In ulcerated IH, initial chemotherapy comprising 2 mg/kg β-blockers daily until 6 months after wound healing resulted in complete wound healing and marked involution in a 3 year-old girl [5].

Vascular malformations

Vascular malformations consist of CM, VM, LM, and AVM. Combinations of more than one malformation are categorized as complex vascular malformations and complex syndromes, such as Klippel–Trénaunay syndrome (CM + VM + LM) or Parkes Weber syndrome [AVM/or arteriovenous fistula (AVF) + skin pseudo-CM + lymphoedema], which presents with more systemic signs and symptoms. Skin necrosis often manifests in severe AVM, combined CM + LM, and a minority of cases of IH.

Assessment and imaging tools

Many imaging tools are able to determine the diagnosis of vascular malformations; however, relevant clinical signs and manifestations are also sought to enable a definitive diagnosis. Less invasive methods are usually applied first, but it is very important to evaluate the vascularity and dynamic changes using angiography in AVMs.

Conventional X-rays

Radiography is usually of little or no value in most cases. VMs may be diagnosed if phleboliths (vascular stones) are observed on plain X-rays. Bone distortion is only seen in large malformations with a soft-tissue mass effect. Some diffuse and massive VMs cause osteolytic lesions and generate a risk of pathological fractures. AVMs involving bone sometimes lead to osteolytic lesions due to intra-osseous nidus formation, which forms owing to arteriovenous shunting or large draining venous channels after the nidus.

Duplex Doppler ultrasonography

Duplex Doppler ultrasonography is primarily used as the initial diagnostic tool [6]. It permits distinction between vascular tumours and malformation, and it also provides information regarding anatomical location. It demonstrates that the lesion is either cystic or tissular, clarifies the presence or absence of flow, and thus, distinguishes between fast-flow and slow-flow malformations, as well as intensity and direction of the flows. Angiostructure and vessel density can be assessed; however, frequently with poor reliability. Peak flow velocities and arterial output may be measured in AVMs. In a head and neck or an extremity AVM, comparing arterial output on the normal side with the abnormal contralateral side is crucial in prognosis, especially possible cardiac failure, and is thus useful for follow-up of AVMs.

CT

CT is of limited use, even after enhancement using intravenous iodinated contrast media; the information provided is limited to indicating whether a lesion is highly vascularized or not. Precise delineation and diagnosis of soft-tissue lesions remain poor with the exception of macrocystic LMs, whereby cysts are clearly depicted. The presence of phleboliths may lead to a diagnosis of VM as distinctive calcifications develop on thrombosis and debris as a result of slow flow. Bony displacement or alteration can be seen due to chronic (long-term) compression, which is seen in both VMs and LMs. Pathological fractures and absorption may be seen in bone or bone-adjacent AVMs.

Figure 5 VMs in the face and neck. A: A 62-year-old woman with VM in the face and neck (lip, tongue, oral floor, neck). Arrow indicates ulceration due to the tight contact with the swollen oral cavity and lip (vermillion). B: At 6 months after the second course of ultrasonic-guided sclerotherapy using absolute ethanol. C: At the third course of sclerotherapy, the excessive tissue was surgically removed. D: At 2 years, after the third course of sclerotherapy and surgery. E: Change of VM is visualized using T2-weighed MRI.


A

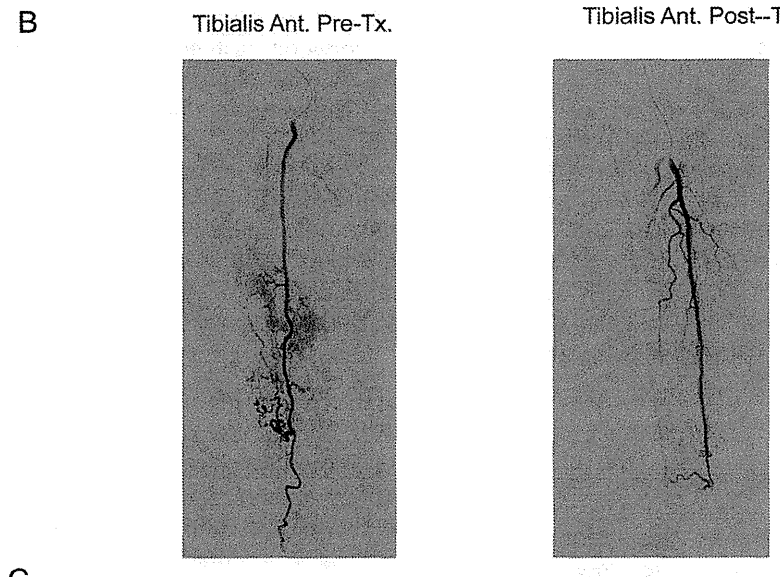
B
Tibialis Ant. Pre-Tx.
Tibialis Ant. Post--Tx.

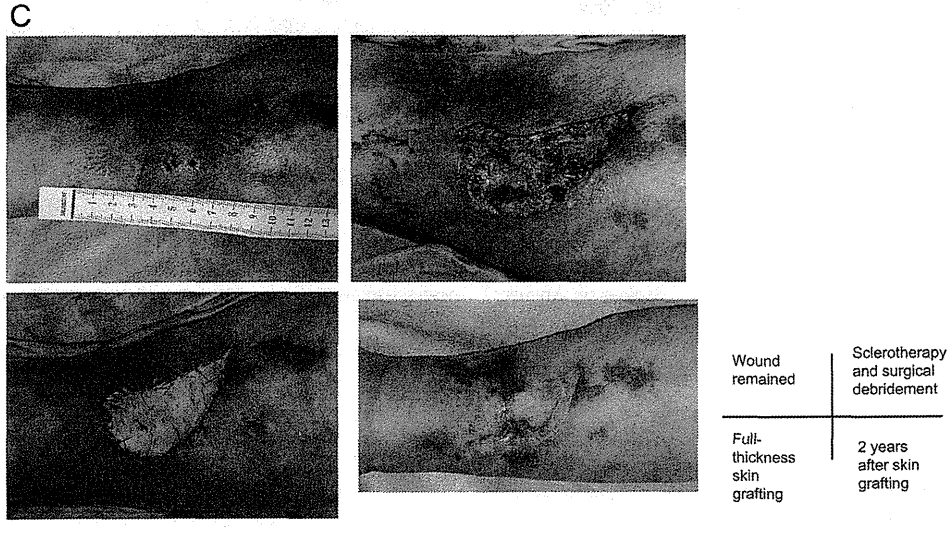
C
Wound remained
Sclerotherapy and surgical debridement
Full-thickness skin grafting
2 years after skin grafting

MRI

MRI is the best diagnostic technique, providing optimal analysis of soft-tissue masses and accurate diagnosis, and can be used to distinguish tissular form cystic lesions, and delineate fast or slow vessel flows. Venous and lymphatic malformations may demonstrate a similar pattern. They are hyperintense on spin-echo T2-weighed sequences and optimally seen in fat-suppression sequences. T1-weighed and fat-suppression sequences with gadolinium injection demonstrate intense enhancement in IH, whereas enhancement is inconsistent and progressive on dynamic sequences in VMs. Gadolinium contrast medium enables differential diagnosis among VMs and LMs. LMs can be distinguished from VMs, as LMs indicate enhancement only at the margins of cysts. By contrast, VMs enhance clearly and homogeneously. MRI is essential before treatment to determine the extent of the lesion and the relationship between the vascular malformation and intact neighbouring nerves and vessels. It is also useful for identification and diagnosis of the lesion. In fast-flow vessels, they are identified as flow voids.

Magnetic resonance angiography (MRA) can confirm the diagnosis of fast-flow vessels; however, it remains insufficient to accurately depict the nidus of AVMs and for analysis of angiostructures.

Vascular imaging

Vascular imaging is used mainly for fast-flow vascular lesions. Angiography is a superior pretreatment assessment of AVMs, which have characteristic early venous drainage. The angiostructure of an AVM can be obtained by identifying its location, arterial supplying vessels, draining veins, and the relationship with normal neighbouring arteries and veins. Angiography is used for diagnosis of quiescent AVMs, which simulate capillary malformation.

Clinical course and treatment

IH

Typically, IH involutes within a year or so. However, skin sequelae may exhibit telangiectasia, anetoderma (shrink skin), and fibro-fatty residual tissue (Fig. 1). When the lesion is beneath clothing, there is no functional loss or damage, and no further treatment but observation is required, careful and regular check-ups are advised. IHs may occasionally demonstrate ulceration in the plateau (22%) and involution (13%) phases, although this typically occurs during the proliferating phase [3]. Once finally involuted and regressed, if the IH lesion occupies a functional vital organ or is in an aesthetically important exposed area, surgery should be attempted to reconstruct and reduce the size. When the lesion is located in the eye, the visual acuity may be disturbed and the visual field may be limited. In cases such as these, surgical removal of the involuted and regressed skin in the upper eye and removal of the cheek tissue toward the lateral side is indicated (Fig. 2).

Atypical haemangioma

Some congenital haemangiomas, distinctive of IH, demonstrate a unique clinical course without spontaneous reduction in size even after 4 years (Fig. 3). This predominately occurs with NICH in which findings at duplex Doppler and ultrasound often depict arteriovenous shunting (Fig. 4).

VM

VMs are volume-occupying lesions containing abnormal and enlarged veins [7]. Although the lesion rarely develops an ulcer, a secondary ulcer and subsequent haemorrhage may develop due to the mass and higher pressure on tissues adjacent to the sharp, hard tissue. This occurs principally in lesions located in the oral cavity, tongue, and lip, whereby teeth can lacerate the vermillion border of the lip, with consequent pain and swelling (Fig. 5A, arrow). Serial sclerotherapy can be performed to reduce the volume of the lesion and control the abnormal blood pooling and communication with the surrounding tissues. Better functional and aesthetic outcome can be obtained after removal of excessive tissue and reconstruction (Fig. 5).

Figure 6 A 73-year-old woman with an AVM in the right medial and lateral lower calf. A: Preoperative T2-weighed MRI image. Arrows indicate the nidus due to the AVM. B: Angiogram in the tibialis anterior demonstrated the fast flow and subsequent early entry in the venous drain, indicating the AVMs (left) and after embolization using NBCA to control flow supply and drainage (right). C: Within 24 h after embolization, percutaneous ultrasonic-guided sclerotherapy followed by surgical debridement and skin grafting. The wound remained healed at 2 years.

AVMs

AVMs are the most frequently occurring skin lesion among the vascular malformations. AVM can develop into ulcers during the natural clinical course and as a result of post-therapeutic morbidity from embolization or sclerotherapy, as the blood flow and perfusion in the local tissues are erroneous and unpredictable with [8] or without pre-existing disease [9]. Embolization using N-butyl cyanoacrylate (NBCA) can be used to control flow supply and drainage, and subsequent percutaneous or transcutaneous ultrasonic-guided sclerotherapy within 24 h may generate sufficient reconstruction of the wound bed. Additional sclerotherapy is used to suppress and control vessel malformations that are tiny or invisible at angiography. Surgical debridement and reconstruction are then performed (Fig. 6).

Treatment

Some vascular tumours (haemangiomas) and vascular malformations develop wounds and ulcers. Medication and management will follow clinical and imaging diagnostics. AVMs generally demonstrate the most severe ulcers, but ulcerated IH may produce intractable pain in the perioral region. Topical use of a sealant and systemic corticosteroid may control the pain, with easy access to feeding and healing of the ulcer itself [10]. Corticoids may induce cessation of the patient's growth if used other than during the growing phase of IH [11]. Thus, other agents, such as β-blockers, have recently been used for periods of 2–6 weeks and exhibit earlier wound healing and regression of the tumour [12].

By contrast, in the chronic stasis ulcer, arteriovenous communication resembling the features of AVMs causes rapid-growth ulceration [8]. Skin necrosis is demonstrated on the hands in patients with primary AVM ulcers as well as in 40% of patients after treatment with embolo/sclerotherapy [9].

In AVMs, a practical clinical staging system is proposed, which describes the progression of AVMs proposed by Schobinger [13]. In the initial quiescent stage (stage I), the lesion presents as warm, pink–blue macules. It subsequently expands with pulsations, thrills, and bruits (stage II), and eventually becomes destructive with pain, haemorrhage, or ulceration (stage III). The final stage demonstrates decompensation and results in congestive heart failure (stage IV) [13]. Ideally treatment should commence at stages I and II, but frequently, AVMs will not be detected until stage III, when ulceration is observed as a destructive clinical sign. In the study of Kohout et al., with a mean follow-up of 4.6 years, the cure rate of AVMs was reported as 75% for stage I, 67% for stage II, and 48% for stage III [13]. AVMs are exacerbated after trauma, hormonal change, pregnancy, or puberty. Duplex ultrasonic and clinical signs and symptoms can assist in therapeutic decision-making; however, more precise and effective evaluation using MRI and angiography are necessary. Although MRI can provide insight into the spatial relationship between the lesion and the surrounding tissues and organs, angiography is most important for the assessment of abnormal vasculature and therapeutic evaluation when embolization is required. Embolization is most often necessary for the abolition or reduction of the nidus, which denotes the main lesion of vascular shunting, supplying flow, pooling, and drainage. When AVM lesions are localized, as often seen in stage II, and are distinct from vital organs, either surgical removal alone or combined therapy with precedent embolization within 24–48 h is the initial choice of treatment. If the defect is large, reconstruction will follow [14]. If the lesion is extensive or destructive (stage III) and the lesion is not clearly delineated, controlled attenuation of the lesion should be considered.

Conclusion

The treatment of wounds caused by vascular anomalies involves detailed assessment of the clinical manifestations and imaging data. Control of the pathological abnormal vasculature precedes surgical removal and reconstruction. In vascular tumours, clinical diagnosis and observation are important, whereas extensive imaging is useful in vascular malformations, especially in AVMs.

Conflict of interest

The authors do not hold any conflict of interest in the content of this manuscript.

References

[1] Enjolras O, Mulliken JB. Vascular tumors and vascular malformations. Adv Dermatol 1997;13:375–423.
[2] Wassef M, Enjolrad O. Superficial vascular malformations: classification and histopathology. Ann Pathol 1999;19: 253–64.
[3] Chamlin SL, Haggstrom AN, Drolet BA, Baselga E, Frieden IJ, Garzon MC, et al. Multicenter prospective study of ulcerated hemangiomas. J Pediatr 2007;151:684–9.

[4] Maguiness SM, Hoffman WY, McCalmont TH, Frieden IJ. Early white discoloration of infantile hemangioma: a sign of impending ulceration. Arch Dermatol 2010;146:1235–9.
[5] Cavalli R, Buffon RB, de Souza M, Colli AM, Gelmetti C. Tumor lysis syndrome after propranolol therapy in ulcerative infantile hemangioma: rare complication or incidental finding? Dermatology 2012;224:106–9.
[6] Paltiel HJ, Burrows PE, Kozakewich HP, Zurakowski D, Mulliken JB. Soft tissue vascular anomalies: utility of US for diagnosis. Radiology 2000;214:747–54.
[7] Berenguer B, Burrows PE, Zurakowski D, Mulliken JB. Sclerotherapy of craniofacial venous malformations: complication and results. Plast Reconstr Surg 1999;104:1–11.
[8] Komai H, Kawago M, Juri M. Massive spouting bleeding from chronic stasis ulceration caused by arteriovenous communication of the lower extremity. J Vasc Surg 2006;44:658–9.
[9] Park UJ, Do YS, Park KB, Park HS, Kim YW, Lee BB, et al. Treatment of arteriovenous malformations involving the hand. Ann Vasc Surg 2012;26:643–8.
[10] Strand M, Smidt AC. Pain management for ulcerated infantile hemangiomas. Pediatr Dermatol 2012;29:124–6.
[11] Akhavan A, Zippin JH. Current treatments for infantile hemangiomas. J Drugs Dermatol 2010;9:176–80.
[12] Kim LH, Hogeling M, Wargon O, Jiwane A, Adams S. Propranol: useful therapeutic agent for ulcerated infantile hemangiomas. J Pediatr Surg 2011;46:759–63.
[13] Kohout MP, Hansen M, Pribaz JJ, Mulliken JB. Arteriovenous malformations of the head and neck: natural history and management. Plast Reconstr Surg 1998;102:643–54.
[14] Marler JJ, Mulliken JB. Current management of hemangiomas and vascular management. Clin Plast Surg 2005;32: 99–116.

J Ped Surg Case Reports 1 (2013) 29–31

Contents lists available at SciVerse ScienceDirect

Journal of Pediatric Surgery CASE REPORTS

journal homepage: www.jpscasereports.com

Prenatally detected giant congenital hemangioma of the fetal neck

Shuichiro Uehara [a,b,*], Toshimichi Hasegawa [a], Hiroomi Okuyama [a], Hisayoshi Kawahara [a], Akio Kubota [a], Keigo Osuga [c], Eiichi Morii [d]

[a] Department of Pediatric Surgery, Osaka Medical Center and Research Institute for Maternal and Child Health, Osaka 594-1101, Japan
[b] Division of Pediatric Surgery, Department of Surgery, Osaka University Graduate School of Medicine, Osaka 565-0871, Japan
[c] Department of Diagnostic and Interventional Radiology, Osaka University Graduate School of Medicine, Osaka 565-0871, Japan
[d] Department of Pathology, Osaka University Graduate School of Medicine, Osaka 565-0871, Japan

ARTICLE INFO

Article history:
Received 16 February 2013
Received in revised form
1 March 2013
Accepted 1 March 2013

Key words:
Congenital hemangioma
Antenatally detected
Magnetic resonance imaging

ABSTRACT

Hemangiomas and vascular malformations constitute a variety of non-cancerous birthmarks and lesions. We experienced a rare case of a fetus with a giant congenital hemangioma detected on the fetal ultrasonography and magnetic resonance imaging (MRI). The patient was delivered via a planned cesarean section and underwent extirpation of the tumor on the 16th postnatal day due to concerns of bleeding from the tumor. A pathological examination demonstrated glucose transporter (GLUT)-1-negative lobular capillary proliferation compatible with a diagnosis of congenital hemangioma. The infant was discharged without complications on day 14 after tumor resection. Currently, at 5 years of age, no tumor recurrence has so far been observed since the extirpation. The antenatal images of this case are presented and the perinatal management is discussed.

Congenital hemangiomas (CHs) are fully formed at birth, having undergone proliferation in utero, do not exhibit the typical postnatal evolutive pattern of infantile hemangioma (IH) and can be diagnosed prenatally using ultrasonography [1]. CH is a subtype of benign vascular tumor, that is further characterized as either rapidly involuting (RICH) or non-involuting (NICH). In most infants with RICH, involution is complete, leaving anetodermic skin within 6–14 months of life, whereas NICH lesions grow proportionally with the child's growth. NICHs never disappear and therefore require eventual excision. However, when CH is prenatally detected and there are concerns of bleeding or heart failure due to the high blood flow of the tumor, surgical resection may be performed immediately after birth.

We herein report a rare case of a fetus with a giant congenital hemangioma detected on the fetal ultrasonography and magnetic resonance imaging (MRI) that was treated with surgical resection.

1. Case report

A 29-year-old female was referred at 29 weeks of gestation due to an ultrasonographically detected tumor located on the fetal posterior neck. Ultrasonography revealed a 65 × 67 × 43-mm heterogeneous tumor that made contact with the infant's spine and skull (Fig. 1A). Color Doppler imaging revealed rich vascular formation and blood flow in the tumor. T2-weighted images of magnetic resonance imaging (MRI) obtained at 34 weeks of gestation revealed iso-high signal intensity (Fig. 1B). These findings were compatible with a diagnosis of hemangioma. During the pregnancy, fetal echography showed no increases tumor size; however, a mild right heart load was detected.

At 38 weeks of gestation, a planned cesarean section was performed with appropriate informed consent to prevent dystocia and bleeding from the tumor during vaginal delivery. A 2622-g-male infant was delivered with Apgar scores of 8 and 9 at one and 5 min, respectively. The infant did not require resuscitation or respiratory support. The tumor originated from the posterior of the neck, as observed on prenatal images. The color of the tumor became more red with each passing day, and the surface of the tumor gradually demonstrated enlargement, creating an ulcer on the surface of the tumor (Fig. 2). No signs of involution of the tumor were observed until the 15th postnatal day. Since the tumor appeared ready to bleed from the surface, tumor resection was performed on the 16th postnatal day. First, a spindle-shaped skin incision was made around the tumor. Tumor mobilization was achieved with fine ligations of the vessels in the subcutanous lesion, preserving the posterior neck muscles. The tumor was successfully resected completely. Skin grafting was not required to close the wound. The amount of blood loss was 132 ml, and the operative time was 3 h and 13 min. A pathological examination revealed lobular capillary

* Corresponding author. Division of Pediatric Surgery, Department of Surgery, Osaka University Graduate School of Medicine, 2-2 Yamadaoka, Suita, Osaka 565-0871, Japan. Tel.: +81 6 6879 3753; fax: +81 6 6879 3759.
E-mail address: uehara@pedsurg.med.osaka-u.ac.jp (S. Uehara).

2213-5766/$ – see front matter © 2013 Elsevier Inc. All rights reserved.
http://dx.doi.org/10.1016/j.epsc.2013.03.003

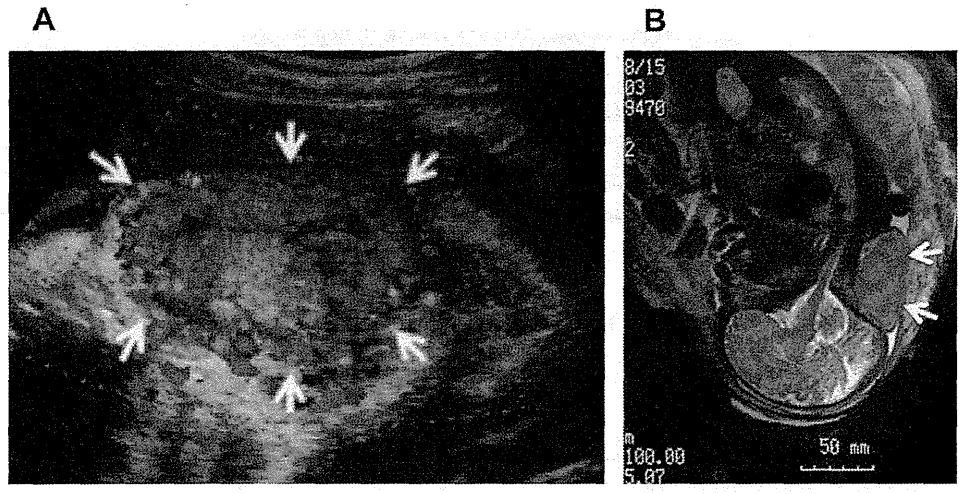

Fig. 1. Prenatal images of color Doppler ultrasonography at 29 weeks of gestation showing the 65 × 67 × 43-mm heterogeneous tumor that made contact with the infant's spine and skull. Rich vascular formation and blood flow in the tumor was observed (A). T2-weighted images of magnetic resonance imaging (MRI) obtained at 34 weeks of gestation revealed iso-high signal intensity (B).

proliferation (Fig. 3A) and a GLUT-1-negative status in the vascular endothelial cells, in contrast to the positive findings in red blood cells observed in the vessels as an internal control of GLUT-1 (Fig. 3B), compatible with a diagnosis of congenital hemangioma. The infant was discharged without complications on day 14 after tumor resection. Currently, at age 5 years of age, no tumor recurrence has not been observed since the tumor resection.

2. Discussion

The concept of a classification system for pediatric vascular anomalies was first established in 1982 based on the pathologic findings reported in a study by Mulliken and Glowacki and later modified by the International Society for the Study Group of Vascular Anomalies [2]. Congenital hemangioma (CH) is a subtype of benign vascular tumor that is further characterized as rapidly involuting (RICH) or non-involuting (NICH). Infantile hemangioma (IH) and CH are distinguished based on their clinical features and the presence of a GLUT-1-positive expression in the endothelial cells of infantile hemangioma (IH) [3]. The involution observed in cases of RICH is very similar to that observed in cases of IH, which regresses slowly after occurring during the first year of life [4]. In contrast, NICH does not exhibit the regression. Consequently, the possibility of NICH being a later stage of RICH has been suggested. Therefore, to determine the fate of RICH and NICH, monitoring for an observation period of a few years and performing serial postnatal imaging can provide insight into imaging evolution and involution of RICH during the first year of life.

Fig. 2. Postnatal photograph showing the neonate with a tumor on the posterior neck.

Both CH and IH appear as fast-flow lesions on ultrasound and exhibit flow voids on MRI. RICH and NICH are more likely to be heterogeneous on US and much more likely to contain identifiable calcification. On MRI, these lesions exhibit high intensity on T2-weighted images and iso-intensity on T1-weighted images; prior to involution, they enhance avidly and homozygously [5]. Fast-flow is also detected in arterial vascular malformations; however, it can be easily differentiated on MRI. Prenatal screening with ultrasonography allows for the early detection of CH as early as 12 weeks of gestation [4]. A distinction between RICH and NICH lesions cannot be made on prenatal ultrasound [6]. If CH is diagnosed antenatally, the lesion can be followed on ultrasonography and MRI to further define the tumor characteristics and monitor growth [7].

In our case, immunohistochemical staining revealed negative GLUT-1 results, suggesting a diagnosis of CH. However, it is difficult to distinguish RICH from NICH before and at birth without the knowledge obtained from histological findings and observation for at least one year. Since the tumor in our case was likely to be injured by mechanical friction, we believed that it should be excised without observation to distinguish involution.

As Nolan et al. [8] previously reported, life-threatening hemorrhage associated with passage through the birth canal can result in by birth trauma if the tumor is large and located on the surface of the neonate. In such cases, cesarean section should be used for delivery. Bleeding may also occur, even after birth, due to mechanical friction. Powell et al. [9] reported that two cases of severe bleeding episodes occurred during the first week of life. Close antenatal evaluation, including the frequent use of US to monitor lesion size and blood flow, should be conducted. Large hemangiomas can cause congestive heart failure due to hyperdynamic circulation leading to increasing cardiac output; therefore, fetal circulatory parameters should also be monitored. When these findings are observed, surgical excision should be considered

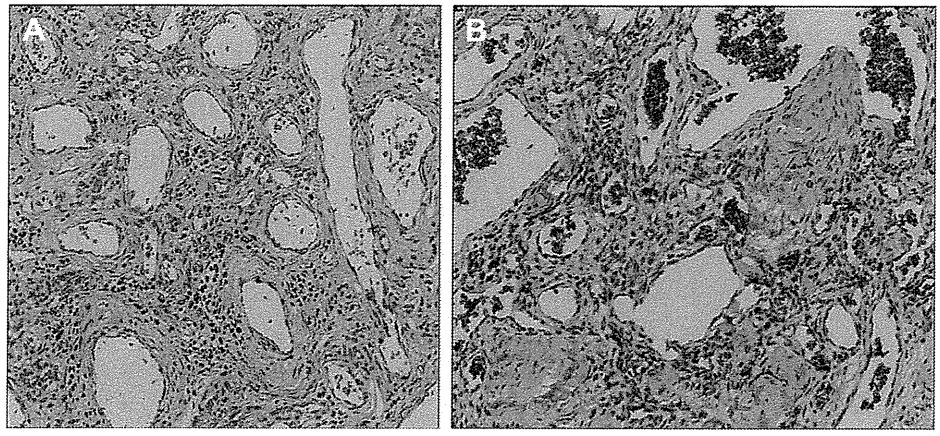

Fig. 3. Microscopic examination showing capillaries and feeding vessels with flattened endothelial cells on hematoxylin eosin staining (A, ×200). GLUT-1 immunostaining was negative (B, ×200), consistent with a diagnosis of congenital hemangioma.

immediately after birth. Otherwise, the first line of treatment should be close observation.

3. Conclusion

We herein reported a rare case of a fetus with a giant congenital hemangioma detected on the fetal ultrasonography and MRI that was treated with the extirpation. Close follow-up before and after birth led to concerns of bleeding after birth, and a surgical approach was ultimately selected.

Conflicts of interest

None.

Sources of funding

None.

Acknowledgement

The authors thank Dr. Brian Quinn, Japan Medical Communication for editing this manuscript.

References

[1] Brix M, Soupre V, Enjolras O, Vazquez MP. Antenatal diagnosis of rapidly involuting congenital hemangiomas (RICH). Rev Stomatol Chir Maxillofac 2007; 108:109–14.
[2] Mulliken JB, Enjolras O. Congenital hemangiomas and infantile hemangioma: missing links. J Am Acad Dermatol 2004;50:875–82.
[3] North PE, Waner M, Mizeracki A, Mrak RE, Nicholas R, Kincannon J, et al. A unique microvascular phenotype shared by juvenile hemangiomas and human placenta. Arch Dermatol 2001;137:559–70.
[4] Berenguer B, Mulliken JB, Enjolras O, Boon LM, Wassef M, Josset P, et al. Rapidly involuting congenital hemangioma: clinical and histopathologic features. Pediatr Dev Pathol 2003;6:495–510.
[5] Gorincour G, Kokta V, Rypens F, Garel L, Powell J, Dubois J. Imaging characteristics of two subtypes of congenital hemangiomas: rapidly involuting congenital hemangiomas and non-involuting congenital hemangiomas. Pediatr Radiol 2005;35:1178–85.
[6] Fadell 2nd MF, Jones BV, Adams DM. Prenatal diagnosis and postnatal follow-up of rapidly involuting congenital hemangioma (RICH). Pediatr Radiol 2011;41: 1057–60.
[7] Ozcan UA. Rapidly involuting congenital hemangioma: a case of complete prenatal involution. J Clin Ultrasound 2010;38:85–8.
[8] Nolan M, Hartin Jr CW, Pierre J, Ozgediz DE. Life-threatening hemorrhage from a congenital hemangioma caused by birth trauma. J Pediatr Surg 2012;47: 1016–8.
[9] Powell J, Blouin MM, David M, Dubois J. Bleeding in congenital hemangiomas: crusting as a clinical predictive sign and usefulness of tranexamic acid. Pediatr Dermatol 2012;29:182–5.

ORIGINAL ARTICLE

Apelin Inhibits Diet-Induced Obesity by Enhancing Lymphatic and Blood Vessel Integrity

Mika Sawane,[1,2] Kentaro Kajiya,[2] Hiroyasu Kidoya,[1] Masaya Takagi,[2] Fumitaka Muramatsu,[1] and Nobuyuki Takakura[1]

Angiogenesis is tightly associated with the outgrowth of adipose tissue, leading to obesity, which is a risk factor for type 2 diabetes and hypertension, mainly because expanding adipose tissue requires an increased nutrient supply from blood vessels. Therefore, induction of vessel abnormality by adipokines has been well-studied, whereas how altered vascular function promotes obesity is relatively unexplored. Also, surviving Prox1 heterozygous mice have shown abnormal lymphatic patterning and adult-onset obesity, indicating that accumulation of adipocytes could be closely linked with lymphatic function. Here, we propose a new antiobesity strategy based on enhancement of lymphatic and blood vessel integrity with apelin. Apelin knockout (KO) mice fed a high-fat diet (HFD) showed an obese phenotype associated with abnormal lymphatic and blood vessel enlargement. Fatty acids present in the HFD induced hyperpermeability of endothelial cells, causing adipocyte differentiation, whereas apelin promoted vascular stabilization. Moreover, treatment of apelin KO mice with a selective cyclooxygenase-2 inhibitor, celecoxib, that were fed an HFD improved vascular function and also attenuated obesity. Finally, apelin transgenic mice showed decreased subcutaneous adipose tissue attributable to inhibition of HFD-induced hyperpermeability of vessels. These results indicate that apelin inhibits HFD-induced obesity by enhancing vessel integrity. Apelin could serve as a therapeutic target for treating obesity and related diseases. ***Diabetes* 62:1970–1980, 2013**

Obesity appears to be associated with a combination of genetic susceptibility, increased consumption of high-energy foods, and decreased physical activity, leading to excessive accumulation of white adipose tissues that serve to store surplus energy in the form of lipid within adipocytes (1). It is correlated with type 2 diabetes, cardiovascular disease, and certain types of cancer, and therefore represents a serious public health problem. Although the molecular mechanisms underlying obesity have not been fully clarified, effective therapeutic approaches are needed.

The blood and lymphatic systems are composed of dense networks of capillaries. Blood vessels are indispensable to import and carry fluid, dissolved proteins, and cells into interstitial space, whereas lymphatic vessels drain protein-rich lymph and traffic immune cells from the extracellular space (2). Adipose tissue is mainly composed of adipocytes surrounded by stromal vascular tissue. The balance of adipokine production is disrupted by excess adipose tissue, leading to chronic vascular inflammation, which in turn may lead to cardiovascular disease (3). The outgrowth of adipose tissue is tightly correlated with angiogenesis (4). Thus, antiangiogenesis therapy has emerged as a potential treatment of obesity. However, this idea remains controversial not only because angiogenesis is physiologically important but also because brown adipose tissue consumes more energy if angiogenesis is increased (5). Moreover, there is an increasing emphasis on lymphatic function in obesity research. *Chy* mice, a naturally occurring mouse model of lymphedema attributable to heterozygous inactivating mutations in vascular endothelial growth factor receptor (VEGFR)-3, exhibit adipose layer accumulation (6). Also, surviving Prox1 heterozygous mice show abnormal lymphatic patterning and adult-onset obesity (7). Thus, accumulation of adipocytes could be closely linked with the structure and function of lymphatic vessels. However, little is known about how vessel integrity influences adipocyte dynamics.

The apelin gene encodes a 77-amino-acid preprotein, which is cleaved to shorter active peptides that bind to the apelin receptor (APJ), a G-protein-coupled receptor (8). The full-length mature peptide comprises 36 amino acids (apelin-36), and other active fragments, including a 13-amino-acid peptide known as apelin-13, also are formed. Apelin is expressed widely in the vascular endothelium and acts both locally and via endocrine signaling to activate APJ, which is expressed in cardiomyocytes, endothelial cells, and vascular smooth muscle cells (9). Apelin/APJ signaling is located downstream of angiopoietin-1/Tie2 signaling in endothelial cells (10). Apelin transgenic mice develop enlarged, but not leaky, blood vessels in ischemia, leading to functional recovery (11). More recently, we have shown that apelin attenuates edema formation and inflammation by promoting lymphatic function in vivo (12).

Herein, we show that the apelin/APJ system enhances the integrity of lymphatic and blood vessels exposed to dietary fatty acids, resulting in inhibition of high-fat diet (HFD)-induced obesity. These results suggest that apelin may be a new therapeutic target in the treatment of obesity and its related diseases.

RESEARCH DESIGN AND METHODS

Animals. Male and female apelin-deficient mice (knockout [KO]) and apelin transgenic mice under the control of keratin 14 on a C57/BL6 background (K14-apelin) were generated as described previously (11). All animals were housed in groups (n = 3–10) in a temperature-controlled room with a 12-h/12-h light–dark cycle. Both wild-type (WT) and KO mice (7–11 weeks old) were maintained on HFD (D12492, 60 kcal % fat; Research Diets, New Brunswick, NJ) for 17 weeks. In other studies, WT and KO mice fed the same HFD were further divided into two groups (n = 3–7) cotreated with vehicle or 0.1% selective cyclooxygenase (COX) 2 inhibitor celecoxib (CEL; LC Laboratories, Woburn, MA) from the age of 7–8 weeks for 8 weeks. Moreover, K14-apelin and WT mice at age 4–5 weeks were fed HFD (D12451, 45 kcal % fat; Research Diets)

From the [1]Department of Signal Transduction, Research Institute of Microbial Diseases, Osaka University, Osaka, Japan; and the [2]Shiseido Innovative Science Research Center, Yokohama, Japan.
Corresponding author: Kentaro Kajiya, kentaro.kajiya@to.shiseido.co.jp, or Nobuyuki Takakura, ntakaku@biken.osaka-u.ac.jp.
Received 9 May 2012 and accepted 25 January 2013.
DOI: 10.2337/db12-0604

for 8 weeks. Mice had free access to food and water. We measured body weight and the mass of food consumed every week. At the end of the study, we weighed the inguinal and mesenteric fat pads and collected the ears, back skin, and mesenteric fat for histological analysis, and collected blood samples for analysis of the circulating levels of glucose, triglyceride, free fatty acids, HDL cholesterol, insulin, leptin, and adiponectin. Plasma of HR-1 hairless mice fed a regular diet (RD; CRF-1; Oriental Yeast, Tokyo, Japan) or HFD (D12492, 60 kcal % fat; Research Diets) for 11 weeks also was collected. The current study was approved by the Ethics Committee of Shiseido Research Center in accordance with the guidelines of the National Institute of Health.

Immunohistochemical and computer-assisted morphometric vessel analysis. Immunofluorescence analysis was performed on 6-μm cryostat sections of mouse back skin or 12-μm cryostat sections of mesenteric fat using antibodies against the macrophage monocyte marker CD11b (BD Biosciences, Bedford, MA), the blood vessel–specific marker meca-32 (BD Biosciences), the lymphatic-specific marker LYVE-1 (MBL, Nagoya, Japan), podoplanin (AngioBio, Del Mar, CA), APJ (10), perilipin (PROGEN Biotechnik GmbH, Heidelberg, Germany), Ki-67 antigen (Dako Cytomation, Glostrup, Denmark), and corresponding secondary antibodies labeled with AlexaFluor488 or AlexaFluor594 (Molecular Probes, Eugene, OR). Routine hematoxylin and eosin staining also was performed. Sections were examined with an Olympus AX80T microscope (Olympus, Tokyo, Japan) and images were captured with a DP-controlled digital camera (Olympus). Morphometric analyses were performed using the IP-LABORATORY software as described (13). Three different fields of each section were examined and the number of macrophages and the average vessel size in the dermis and in the mesenteric fat were determined. Whole-mount immunohistochemical analysis of ear skin was performed. Tissues were incubated in 30% H_2O_2, 3% normal goat serum (Invitrogen, Camarillo, CA), and 0.25% Triton X-100 in PBS, and incubated overnight at 4°C with anticlaudin-5 antibody (Santa Cruz Biotechnology, Santa Cruz, CA) or anti-CD31 antibody (BD Biosciences), as an endothelial marker, and anti-podoplanin antibody (AngioBio, Del Mar, CA) or anti-LYVE-1 antibody, as a lymphatic marker. Then, corresponding secondary antibodies labeled with AlexaFluor488 or AlexaFluor594 (Molecular Probes) were applied. Specimens were viewed with a LSM5 Pascal confocal laser-scanning microscope (Carl Zeiss, Thornwood, NY).

Adipose tissue imaging. Adipose tissue imaging of inguinal fat was performed as described previously (14). The inguinal subcutaneous fat was minced into small pieces and incubated with BODIPY (4,4-difluoro-3a,4a-diaza-s-indacene) conjugated with Alexa Fluor (Invitrogen-Molecular Probes, Carlsbad, CA) as a lipid droplet marker and Isolectin IB_4 Alexa Fluor dye conjugates (Invitrogen-Molecular Probes) as an endothelial marker. The three-dimensional structure of adipocytes was observed using a LSM5 Pascal confocal laser-scanning microscope (Carl Zeiss). Adipocyte diameter was determined using IPLab software. Four image fields were acquired from three animals in each group, and the diameters of 20 cells in each field were measured by an observer blinded regarding the status of the sample. Adipocytes were defined as regular, round, $BODIPY^+$ cells without plasma membrane disruption.

Blood analysis. Plasma glucose, HDL cholesterol, and triglyceride levels were measured using a Fuji DRI-CHEM analyzer (Fuji Film, Tokyo, Japan). Plasma free fatty acid level was determined with a Wako NEFA C test kit (Wako Chemicals, Neuss, Germany). Insulin, leptin, and adiponectin were assayed with a mouse insulin ELISA kit (Shibayagi, Gunma, Japan) and a leptin and adiponectin ELISA kit (R&D Systems, Minneapolis, MN), respectively, according to the manufacturers' instructions.

Plasma extravasation and lymphatic functional analysis. To examine the blood vascular permeability, Miles assay was performed as previously described (11). Briefly, mice were anesthetized and intravenously injected with 100 μL of a 1% solution of Evans blue dye in 0.9% NaCl. At 30 min after dye injection, pictures were taken and the epididymal fat was removed. The dye was eluted from dissected samples with formaldehyde at 56°C and the optical density was measured by spectrophotometry (Biotrak II; GE Healthcare, Fairfield, CT) at 620 nm. For lymphatic functional analysis, a 1-μl aliquot of 1% solution of Evans blue dye in 0.9% NaCl was injected intradermally at the inner surface of the rim of the ear using a 10-μL Hamilton syringe; this is a standard method to macroscopically visualize cutaneous lymphatic vessels and lymphatic drainage. Mouse ears were photographed at 1 and 5 min after the dye injection. Additionally, 100 μL of 1% solution of Evans blue dye in 0.9% NaCl was injected into the stomach and at 30 min after dye injection, the mesenteric fat was carefully removed from the intestine. The optical density of the eluted dye in the mesenteric fat was measured.

Cells. Human dermal lymphatic endothelial cells (LECs) were isolated from neonatal human foreskins by immunomagnetic purification as described previously (15). Lineage-specific differentiation was confirmed by real-time RT-PCR for the lymphatic vascular markers Prox1, LYVE-1, and podoplanin, as well as by immunostaining for Prox1 and podoplanin as described (13). Human umbilical vein endothelial cells were purchased (PromoCell, Heidelberg, Germany) and cultured in endothelial basal medium (Lonza, Verviers, Switzerland) with supplements provided by the suppliers for up to 11 passages. Primary human subcutaneous preadipocytes (Lonza) were cultured as recommended by the supplier in preadipocyte basal medium 2 containing 10% FBS, 2 mmol/L L-glutamine, and antibiotics. The 3T3-L1 preadipocytes were cultured in DMEM with 10% FBS and antibiotics.

Permeability assay. LECs and human umbilical vein endothelial cells were grown to confluence on the fibronectin-coated surface of 0.4-μm pore-size tissue culture inserts (Corning, Lowell, MA). Oleate (20 or 100 μmol/L) and steareate (20 or 100 μmol/L) were placed into the upper and lower chambers for 5 h after incubation with apelin-13 (1,000 ng/mL) or a selective COX2 inhibitor, CEL (1 μmol/L), for 1 h. FITC-dextran was added to the upper chambers, and the apparatus was then placed in a CO_2 incubator at 37°C. After incubation for 15 min, a 100-μL sample was taken from the lower chamber and the absorbance of FITC-dextran was determined at 492 nm using a spectrophotometer (Fluoroskan Ascent; Thermo Fisher Scientific, Waltham, MA).

Adipocyte differentiation assay. Differentiation of 3T3-L1 preadipocytes was performed by treatment with insulin, dexamethasone, and 3-isobutyl-1-methylxanthine in DMEM with 10% FBS for 2 days as described (16). Then, the medium was replaced with DMEM containing 10% FBS and insulin before coculture with LECs. Coculture was performed by incubating LECs to confluence on the 0.4-μm pore-size cell culture insert (Corning) and placing them in 6-well plates containing 3T3-L1 adipocytes differentiated for 2 days; 0.5% plasma from mice fed RD or HFD for 11 weeks was added to the upper chambers. After incubation for 7 days, the cells in the lower wells were stained with Oil-Red-O (Wako Pure Chemical Industry, Osaka, Japan) as described previously (17). The stained lipids present in the mature adipocytes were solubilized with isopropanol and measured spectrophotometrically at 510 nm. To induce differentiation of human preadipocytes into mature adipocytes, confluent preadipocytes in plates were cultured in preadipocyte basal medium 2 plus 10% FBS, 2 mmol/L glutamine, and antibiotics for 2 days and then switched to preadipocyte basal medium 2 plus 10% FBS, 2 mmol/L glutamine, antibiotics, 10 μg/mL insulin, 500 μmol/L isobutylmethylxanthine, 1 μmol/L dexamethasone, and 200 μmol/L indomethacin in the presence or absence of oleate (100 μmol/L) and steareate (100 μmol/L). After 9 days of incubation, cells were fixed with 10% formaldehyde, stained with Oil-Red-O (Wako Pure Chemical Industry) and observed under a bright-field microscope (Olympus) as described previously (17).

Immunofluorescence microscopy. LECs and human umbilical vein endothelial cells were seeded on cover slips and incubated until confluence. For the detection of VE-cadherin, cells were fixed with 1% PFA and incubated with anti-VE-cadherin antibody (R&D Systems, Minneapolis, MN). AlexaFluor594-labeled secondary antibody was used for fluorescence detection. All images were acquired using a DP-controlled digital camera (Olympus) on an Olympus AX80T microscope (Olympus).

Quantitative real-time RT-PCR. Total RNAs were isolated from LECs cultured in the presence or absence of apelin (1,000 ng/mL) for 4 h after serum starvation. The expression of COX2 mRNA was examined by quantitative real-time RT-PCR using a LightCycler 480 (Roche Applied Science, Indianapolis, IN). The primers for COX2 were as follows: forward primer, 5′- TAGAGCCCTTCCTCCTGTGC-3′, and reverse primer, 5′- CTGGGCAAAGAATGCAAACA-3′. Expression levels were normalized with respect to β-actin as an internal control (forward primer: 5′-TCACCGAGCGCGGCT-3′; reverse primer: 5′-TAATGTCACGCACGATTTCCC-3′).

Statistical analysis. All data are expressed as means ± SD and as the statistical significance of differences with an unpaired *t* test.

RESULTS

Disruption of apelin/APJ signaling in vivo promotes obesity. To investigate the physiological role of apelin in obesity, apelin KO mice were fed HFD. Surprisingly, after 5 weeks of HFD, apelin KO mice showed increased body weight compared with WT littermates (Fig. 1*A*); at the end of the feeding period, the body weight gains were 20 ± 0.5 g for WT mice and 30 ± 0.5 g for apelin KO mice ($P < 0.01$) (Fig. 1*B*). As expected, both inguinal subcutaneous and mesenteric fat depots were significantly increased by HFD in apelin KO mice compared with WT mice (Fig. 1*C*, *D*). Moreover, hematoxylin and eosin staining revealed a thickened subcutaneous adipose layer in the skin of HFD-fed apelin KO mice as compared with WT mice (Fig. 1*E*). To visualize the three-dimensional structure of adipose tissue, we used fluorescence staining with BODIPY, which recognizes intercellular lipid droplets in